

Survey of the class of isovalent antiperovskite alkaline-earth pnictide compounds

Wen Fong Goh and Warren E. Pickett

Department of Physics, University of California, Davis, California 95616, USA



(Received 10 October 2017; published 4 January 2018)

The few reported members of the antiperovskite structure class $Ae_3Pn_A Pn_B$ of alkaline-earth ($Ae = \text{Ca, Sr, Ba}$) pnictide ($Pn = \text{N, P, As, Sb, Bi}$) compounds are all based on the B -site anion $Pn_B = \text{N}$. All can be categorized as narrow-gap semiconductors, making them of interest for several reasons. Because chemical reasoning suggests that more members of this class may be stable, we provide here a density functional theory (DFT)-based survey of this entire class of $3 \times 5 \times 5$ compounds. We determine first the relative energetic stability of the distribution of pairs of Pn ions in the A and B sites of the structure, finding that the B site always favors the small pnictogen anion. The trends of the calculated energy gaps versus the Ae cation and Pn anions are determined, and we study effects of spin-orbit coupling as well as two types of gap corrections to the conventional DFT electronic spectrum. Because there have been suggestions that this class harbors topological insulating phases, we have given this possibility attention and found that energy gap corrections indicate the cubic structures will provide at most a few topological insulators. Structural instability is addressed by calculating phonon dispersion curves for a few compounds, with one outcome being that distorted structures should be investigated further for thermoelectric and topological character. Examples of the interplay between spin-orbit coupling and strain on the topological nature are provided. A case study of Ca_3BiP including the effect of strain illustrates how a topological semimetal can be transformed into a topological insulator and Dirac semimetal.

DOI: [10.1103/PhysRevB.97.035202](https://doi.org/10.1103/PhysRevB.97.035202)

I. INTRODUCTION

Oxide-based perovskites are the most studied class of ternary compounds for several reasons. First, oxygen is abundant, and a great deal is known about oxide chemistry. Second, the basic cubic structure ABO_3 is simple and is governed to a great extent by ionic bonding. Third, given the near-universal valence state O^{-2} , the A and B cation valences must total six, leaving a large number of combinations, 1:5, 2:4, 3:3, 4:2, 5:1, considering the number of atoms that can assume these formal valences. Most importantly perhaps is the vast range of properties displayed by oxide perovskites, including high-temperature superconductivity; very unusual magnetism; charge, spin, and orbital ordered phases; large linear responses (viz., Born effective charges that can differ by a factor of 2 or more from the formal charge); and multiferroic states, among others.

Halide-based perovskites, viz., KMnF_3 with a monovalent anion, are a closely related class of materials. They are much less prevalent because only 1:2 and 2:1 cation charge pairs are possible, and the higher electronegativity makes synthesis less straightforward. Less common still are nitrogen-based perovskites because the N^{-3} ion requires cations with formal charge pairs 4:5 or 3:6; higher formal valences are rare. N-based perovskites have been the topic of a high-throughput computational study to determine stable examples [1].

Within a given crystal structure it is uncommon, but possible, to interchange the anion and cation sites. The *antiperovskite* class discussed here will be denoted Ae_3AB , where Ae is the (alkaline-earth) cation on the oxygen site and A and B are anions that provide charge balance. Anion formal valences are practically limited to 1, 2, and 3, constraining considerably the cation valences. In this paper we will focus

on divalent alkaline-earth cations, for which the anion formal charges must sum to six, so it can be expected that nearly all of such antiperovskite compounds will have two trivalent anions. Here we consider the class in which both A and B anions are from the pnictogen column of the periodic table. Given the formal charge balance between divalent cations and trivalent anions, this class can be anticipated to harbor insulators and perhaps semimetals. Sun and coauthors have proposed that topological insulating phases may arise in the Ae_3BiN group with application of uniaxial strain [2], providing additional current interest.

Examples of alkaline-earth pnictide antiperovskite compounds have been reported. Some crystallize in cubic structure [3], while others show structural distortions [4] or even form distinct structures; for example, the two compounds Ba_3XN , where $X = \text{Sb}$ and Bi , assume the hexagonal antiperovskite structure [5], suggested to be due to the presence of large-radius alkaline-earth ions. The electronic state of this class of materials is insulating, ranging from relatively wide gap insulating to narrow gap semiconducting. The reported compounds will be discussed in Sec. III D in relation to our results. Notably, compounds in this class with pnictides other than N inside the octahedron have not been reported.

Density functional theory (DFT)-based study of insulating Ca_3BiN and its metallic sister compound Ca_3PbN provided the underlying electronic structure (as shown in the current paper) of this class of materials [6]. DFT-based results for the band structure and selected properties (primarily band gap, elastic, and thermoelectric) have been reported for several of these compounds, which are discussed in Sec. III D. Motivated by the relatively few known examples and the broad possibilities for new materials with important properties, we have carried out a survey of the entire class of $3 \times 5 \times 5$ alkaline-earth

pnictide antiperovskite compounds, viz., $Ae_3Pn_A Pn_B$, where $Ae = \text{Ca, Sr, Ba}$ and $Pn_A, Pn_B = \text{N, P, As, Sb, Bi}$, using first-principles DFT methods. The conventional ordering of atoms Pn_A and Pn_B will follow that of a perovskite with the general chemical formula ABO_3 , where the A cation is twelfold cuboctahedral coordinated and B is sixfold coordinated by an octahedron of O anions. In the case of antiperovskite $Ae_3Pn_A Pn_B$, Pn_B is inside the Ae_6 octahedron, while Pn_A sits in the more open A site.

This paper is organized as follows. The computational methods are summarized in Sec. II. Section III contains many of the basic results and includes a general analysis of the common features of these antiperovskites, the correction to DFT band gaps that are important for small- (or negative-) gap compounds, and a synopsis of previously reported or predicted members of this class. The small or negative gaps bring about the possibility of topological character [7] and the favorable candidates are described in Sec. IV, with a focus on the effects of uniaxial strain. Tuning to topological phases by strain has been an area of growing interest, viz., in Heusler compounds [8], in the HgTe class of compound semiconductors [9], and in the antiperovskite Dirac material Ca_3PbO [10], due to the possibility of enforcing strain by growing films on substrates with appropriate lattice constants. Section V addresses the question of structural stability with two examples, and a concise summary is given in Sec. VI.

II. COMPUTATIONAL METHODS

To study the electronic structure of these 75 compounds, the generalized gradient approximation (GGA) exchange-correlation functional of Perdew-Burke-Ernzerhof-1996 [11] was used, as implemented in the full-potential local orbital (FPLO) [12] scheme. Self-consistency was obtained on a dense k mesh of $20 \times 20 \times 20$ to ensure good convergence of the density and therefore the eigenvalues. The fully relativistic Dirac four-component equations implemented in FPLO were performed to include spin-orbit coupling (SOC) and other relativistic corrections. The cubic lattice constants were obtained by minimizing the energy with respect to volume.

In small-gap compounds, especially for potential topological materials where gaps are typically quite small, the underestimate of the band gap by the GGA functional must be dealt with. We have calculated band gap corrections of the $Ae_3\text{Bi}Pn_B$ subclass using the modified Becke-Johnson (mBJ) exchange-correlation potential. This scheme provides a self-energy-like correction to eigenvalues that has been found to be realistic for several semiconductors and insulators [13–15]. A formally well justified means of obtaining self-energy corrections is provided by GW approximation [16,17]. We have used the FHI-GAP implementation [16] in the WIEN2K code [18] on four compounds, and we make a comparison with the mBJ results in Sec. III C. In this GW_0 implementation the eigenvalue in G_0 is iterated to self-consistency, hence our use of the terminology GW_0 throughout. The linearized augmented plane-wave basis was specified by $R_m G_{\max} = 7$, where R_m is the minimum radius of the atomic spheres and G_{\max} is the largest reciprocal lattice vector. For the GW_0 version of GW implemented in FHI-GAP, the mixed-basis quality was determined by $\ell_{\max} = 3$, $Q = 0.75$. Unoccupied states up to

1000 eV were summed over, the number of discrete imaginary frequency points was 16, and the k -point mesh was $3 \times 3 \times 3$. Increasing the latter to $4 \times 4 \times 4$ resulted in self-energy changes of the order of 0.01 eV.

III. ANALYSIS OF CUBIC STRUCTURES AND SPIN-ORBIT COUPLING

A. Cell volume and energetic stability

The cubic antiperovskite $Ae_3Pn_A Pn_B$ structure [5] (space group $Pm\bar{3}m$) has an Ae_6Pn_B octahedron, with Pn_A surrounded symmetrically by eight octahedra, with the primitive cell pictured in Fig. 1(a). For the cubic (undistorted) structure, the equilibrium lattice constant has been obtained for all $3 \times 5 \times 5$ combinations. These results and the following data are presented in Table I. First is a comparison of the energy difference ΔE upon interchange $Pn_A \leftrightarrow Pn_B$ of the two Pn ions. It is always the case that it is energetically favorable to have the smaller Pn ion in the Pn_B octahedron position. Energy differences, which range from 0.2 to 4.3 eV, are largest when N is one of the ions, and the magnitude of the difference increases with the difference in the atomic number of the anions.

To understand the trends more clearly, in Fig. 2 the values of ΔE are plotted for all pairs versus the lattice constant, which always increases as the size of either the cation or the anion increases. The changes are very regular with the change in the cation and less regular with the change in the anion pair. The overall trend is that the energy difference decreases as the lattice constant increases.

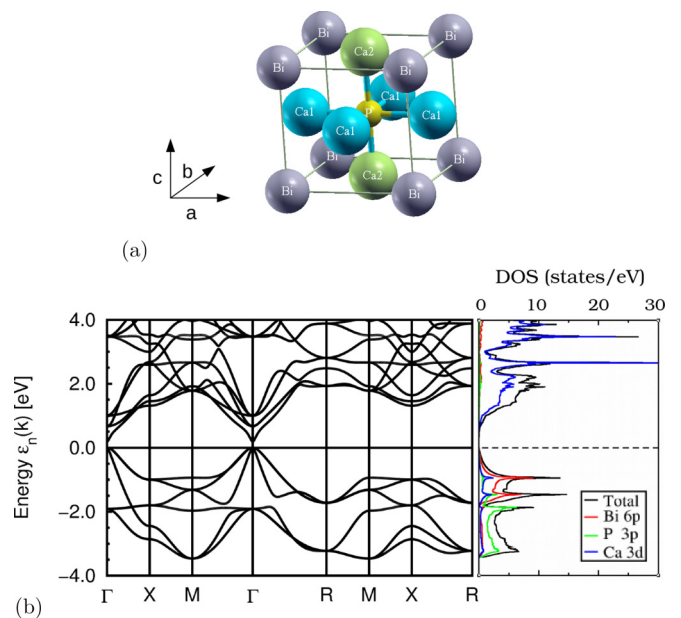


FIG. 1. (a) The antiperovskite structure of Ca_3BiP with tetragonal compression along (001); the space group becomes $P4/mmm$. Ca^{2+} ions lie on two nonequivalent sites (blue and green). (b) Band structure and density of states of cubic Ca_3BiP , without SOC. P 3p bands provide the lowest-valence states, while Bi 6p bands comprise the highest-valence states. Ca 4s and 3d orbitals dominate the lower-conduction states. The gap of 0.2 eV occurs at Γ ; throughout the rest of the zone the gap is large.

TABLE I. Data on the complete class of $Ae_3Pn_A Pn_B$ antiperovskites. a (Å) gives the optimized lattice constants. $\Delta E = E_{Ac_3Pn_A Pn_B} - E_{Ac_3Pn_B Pn_A}$ provides the energy difference (in eV). Since this energy difference is antisymmetric across the diagonal, the energy differences are shown only in the lower left triangle for the stable phase (the smaller Pn ion is always Pn_B). ϵ_g and ϵ_g^{SOC} give the band gap (without and with SOC; in eV), with either a small positive or negative (negative indirect band gap) value, with an exception of a few with bands crossing at the Fermi level or gapless states (represented by SM for the semimetallic state and M for the metallic state). Only the $\nu_0 Z_2$ index is provided because all $\nu_{1,2,3}$ are zero. Values in bold indicate a topological semimetal state.

	N_B						P_B						As_B						Sb_B						Bi_B							
	a (Å)	ΔE (eV)	ϵ_g (eV)	ϵ_g^{SOC} (eV)	Z_2	Z_2	a (Å)	ΔE (eV)	ϵ_g (eV)	ϵ_g^{SOC} (eV)	Z_2	Z_2	a (Å)	ΔE (eV)	ϵ_g (eV)	ϵ_g^{SOC} (eV)	Z_2	Z_2	a (Å)	ΔE (eV)	ϵ_g (eV)	ϵ_g^{SOC} (eV)	Z_2	Z_2	a (Å)	ΔE (eV)	ϵ_g (eV)	ϵ_g^{SOC} (eV)	Z_2	Z_2		
N_A	Ca 4.61	0	0	0	1	5.29	SM	5.42	0	0	1	5.76	-0.01	0	0	1	5.76	-0.01	5.85	-0.01	0	0	1	5.85	-0.01	0	0	1	5.85	-0.01	0	1
	Sr 4.99	0	0	0	1	5.67	0	5.80	0	0	1	6.13	-0.02	0	-0.01	1	6.13	-0.02	6.23	-0.02	0	-0.03	1	6.23	-0.02	0	-0.05	1	6.23	-0.02	0	1
	Ba 5.33	SM	SM	SM	1	6.03	-0.04	6.18	-0.05	0	1	6.52	-0.07	-0.05	-0.06	1	6.52	-0.07	6.61	-0.05	0	-0.08	1	6.61	-0.05	0	-0.12	1	6.61	-0.05	0	1
P_A	Ca 4.73	-2.96	0.85	0.85	0	5.31	0.33	5.42	0.31	0	5.74	0.10	0.05	0	5.74	0	0	1	5.82	0	0	0	1	5.82	0	0	0	1	5.82	0	0	1
	Sr 5.09	-2.55	0.45	0.45	0	5.67	0	5.79	0	1	6.09	0	0	0	6.09	0	0	1	6.17	0	0	0	1	6.17	0	0	0	1	6.17	0	0	1
	Ba 5.43	-2.28	SM	SM	0	6.02	0.03	6.14	0.01	1	6.44	0	0	0	6.44	0	0	1	6.53	0	0	0	1	6.53	0	0	-0.10	1	6.53	0	0	1
As_A	Ca 4.78	-3.38	0.77	0.72	0	5.34	-0.55	5.45	0.09	0	5.75	0	0	0	5.75	0	0	1	5.84	0	0	0	1	5.84	0	0	0	1	5.84	0	0	1
	Sr 5.13	-2.93	0.30	0.28	0	5.70	-0.50	5.81	0	1	6.11	0	0	0	6.11	0	0	1	6.19	0	0	0	1	6.19	0	0	-0.01	1	6.19	0	0	1
	Ba 5.47	-2.64	SM	SM	0	6.04	-0.46	6.16	0	1	6.46	0	0	0	6.46	0	0	1	6.54	0	0	-0.02	1	6.54	0	0	-0.14	1	6.54	0	0	1
Sb_A	Ca 4.88	-4.26	0.46	0.35	0	5.39	-1.76	5.49	0.50	0	5.78	-1.2	0.40	0.22	0	5.78	0.07	0	5.86	0	0	0	1	5.86	0	0	0	1	5.86	0	0	1
	Sr 5.22	-3.77	0.20	0.15	0	5.74	-1.58	5.84	0.16	0	6.13	-1.08	0.10	0	6.13	0	0	1	6.21	0	0	0	1	6.21	0	0	0	1	6.21	0	0	1
	Ba 5.55	-3.40	SM	SM	0	6.08	-1.45	6.19	0.18	0	6.48	-0.99	0.13	0	6.48	0	0	1	6.55	0	0	0	1	6.55	0	0	-0.12	1	6.55	0	0	1
Bi_A	Ca 4.92	-4.35	0.48	0.07	0	5.42	-1.99	5.53	0	1	5.81	-1.44	0	-0.03	1	5.81	-0.29	0	5.89	0	0	-0.10	1	5.89	0	0	-0.12	0	5.89	0	0	1
	Sr 5.26	-3.86	0.25	0.01	0	5.77	-1.75	5.88	-1.26	0	6.15	-1.26	0	-0.05	1	6.15	-0.20	0	6.23	0	0	-0.10	1	6.23	0	0	-0.13	0	6.23	0	0	1
	Ba 5.59	-3.47	SM	SM	0	6.11	-1.61	6.22	-1.17	0	6.50	-0.21	0	-0.10	1	6.50	-0.21	0	6.58	0	0	-0.18	1	6.58	0	0	-0.17	0	6.58	0	0	1

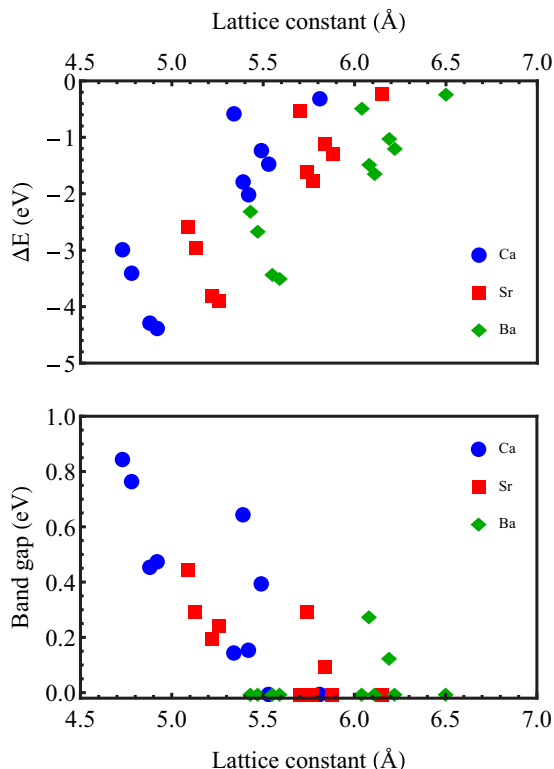


FIG. 2. Top: the energy difference when switching the pnictide ions in $Ae_3Pn_A Pn_B$, plotted versus lattice constant a . Bottom: energy gap (before including spin-orbit coupling) for each pnictide pair, plotted versus lattice constant a ; zero gap indicates a zero-gap semiconductor degeneracy at Γ . In each case the values cluster in groups of four, three, two, and one, corresponding to the lengths of the columns in Table I below the diagonal.

These trends can be understood from Coulomb energetics: if the smaller anion is surrounded by the cation octahedron, the attractive Coulomb energy will be larger. An additional factor is that the A site naturally accommodates a bigger atom than the B site does, giving better volume filling by atoms. The other data in Table I will be discussed below.

B. Electronic band structure

For general orientation, the electronic structure and DOS of a representative compound, Ca_3BiP , containing the largest and the next-to-smallest pnictide ions, is shown in Fig. 1(b). A generic feature in this class of perovskites is that the smaller Pn_B p bands lie lower than the Pn_A p bands, making the larger ion (which, conveniently, also has the largest SOC) the one of interest in determining the band gap (or not) and, subsequently, the topological character. Since both A and B sites have cubic symmetry, both Pn p -band complexes have threefold degeneracy at the Γ point when SOC is neglected, and SOC separates the eigenvalues into $p_{1/2}$ and $p_{3/2}$ states, with the latter for Pn_B forming the top of the valence bands.

In the conduction bands three sets of five Ae d bands dominate. Unexpectedly, a “free-electron-like” band that has no single dominant orbital character, discussed below, lies near the bottom of the conduction bands at Γ and often is the band at the conduction-band minimum (CBM). Since the Ae site

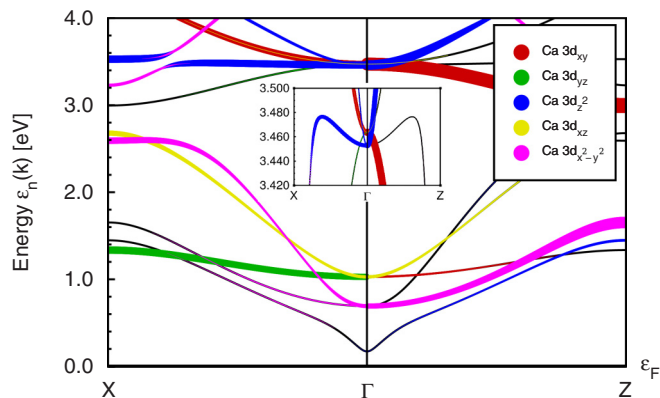


FIG. 3. Color plot differentiating orbital character, showing the band ordering of 3d orbital energies of the apical Ca ions located at $(\frac{1}{2}, \frac{1}{2}, 0)a$ in the unit cell. The inset provides an enlargement of the complex near Γ around 3.5 eV, showing that the d_{xy} and d_{z^2} levels are nearly degenerate at Γ .

has tetragonal symmetry, the d shell is split by the crystal field into a d_{xz}, d_{yz} doublet and three singlets, $d_{xy}, d_{x^2-y^2}, d_{z^2}$, relative to the local (z) axis. For some purposes it would be important to consider how these 30 orbitals on six Ae ions form molecular orbitals on the $Pn_B Ae_6$ octahedron. Actually performing and applying such a transformation are complicated by the fact that each Ae ion’s orbitals are shared with two octahedra.

One fundamental interaction at and near Γ is that of the Pn_A p states with the d orbitals of the 12 Ae ions coordinating it and with the diffuse “ s ” band. To assist in understanding the ordering of the Ae d characters at the Γ point, the orbital characters in the d -band region of the apical Ca ion (whose local axis is along the \hat{z} direction) are plotted in Fig. 3. Ca d_{xy} and d_{z^2} have orbital density oriented towards the four nearest Bi^{-3} ions and two nearest P^{-3} ions, respectively, and their orbital energies are close and are higher than for the other d orbitals. The $d_{x^2-y^2}$ orbital lies lowest in energy, corresponding to an orbital density directed between negative ions, being lower than the highest d orbital by 2.8 eV. This separation changes to 3.6 and 3.3 eV by replacing Ca with Sr and Ba, respectively. The degenerate d_{xz} and d_{yz} orbitals lie about 0.4 eV above the $d_{x^2-y^2}$ orbital. The Pn_A p bands approach and mix with the Ae d bands around the Γ point, with a substantial band gap throughout the rest of the zone.

Trends in band gaps. We here review the behavior of the gaps of the more stable members, which lie in the lower left triangle of Table I. We consider the bands without SOC, from which it is simpler to derive chemical trends. For better understanding the values are plotted in the bottom panel in Fig. 2. For N_B (N on the B site), the Ca compounds have gaps that decrease from 0.85 to 0.48 eV for the progression from P_A to Bi_A . The corresponding Sr compounds have smaller gaps, 0.45 to 0.25 eV, and for the Ba compounds there is band overlap (negative overlap). Moving to P_B and on to Bi_B , there is no monotonic progression of gaps, but there is a clear trend to smaller or zero gaps as the B site atom becomes heavier. Evidently, SOC, which splits the valence-band maximum (VBM), will decrease the gap size and in some cases lead to gap inversion (reported in Table I as zero gap or negative indirect gap).

TABLE II. Inversion energy and band gap of Ae_3BiPn , where $Ae = Ca, Sr, Ba$ and $Pn = N, P, As, Sb, Bi$ with SOC and mBJ correction. The mBJ effect is defined as the difference between the presence and absence of mBJ.

Ae	Property	Pn											
		N			P			As			Sb		
		SOC	SOC + mBJ	mBJ effect	SOC	SOC + mBJ	mBJ effect	SOC	SOC + mBJ	mBJ effect	SOC	SOC + mBJ	mBJ effect
Ca	Inversion energy	0.572	1.587	1.015	-0.283	0.460	0.743	-0.533	0.188	0.721	-0.754	-0.149	0.604
	Band gap	0.081	0.706	0.625	0	0.460	0.460	0	0.188	0.188	0	0	0
Sr	Inversion energy	0.133	1.138	1.005	-0.458	0.286	0.744	-0.658	0.063	0.721	-0.831	-0.226	0.605
	Band gap	0.088	0.746	0.658	0	0.286	0.286	0	0.063	0.063	0	0	0
Ba	Inversion energy	0.003	1.010	1.007	-0.264	0.464	0.727	-0.427	0.283	0.709	-0.633	-0.034	0.599
	Band gap	0	0.483	0.483	0	0.464	0.464	0	0.283	0.283	0	0	0

Topological character: One of the motivations of this survey of 75 compounds was to begin to assess the likelihood of finding topological insulating and also topological semimetal phases in these antiperovskites. We return to this topic in Sec. IV. However, in Table I we have provided the Z_2 topological index for the compounds and structures we have studied for the GGA + SOC bands. In the lower left subdiagonal of Table I, which contains the more stable ordering of the Pn_A, Pn_B pairs, we find no topological bands in the N_B column. However, moving to the heavier Pn_B columns, many $Z_2 = 1$ results are obtained. The profusion of these values appears at first sight to promote optimism. There are important caveats, however. First, GGA calculations are known to underestimate band gaps in insulators. Self-energy corrections to the gap are discussed in Sec. III C. Second, the stability of these model compounds is an issue. Only a few have been reported, which we discuss in Sec. III D. Some may be thermodynamically unstable with respect to more stable phases, while other may be dynamically unstable and distort to a lower-symmetry structure with an altered electronic structure. We return to the question of topological character in Sec. IV.

C. Energy gap correction

We define the inversion energy as the energy of the diffuse s band minus the energy of the VBM (which is that of the A site p band and has negative parity). (In the case where the B site atom is N, the VBM is a strong admixture of Pn_A and N p character.) A negative inversion energy indicates the band inversion that is essential for topological character. Table II provides the inversion energy and band gap for GGA + SOC eigenvalues, with and without mBJ. Note that the band gap, once SOC is included, usually appears away from the Γ point and thus is not equal to the inversion energy. The effect of including mBJ is a separation of conduction bands from valence bands (inversion energy) of 1.0, 0.7, 0.7, and 0.6 eV for N, P, As, and Sb, respectively, a very systematic trend independent of the cation Ca, Sr, and Ba. The final (GGA + mBJ + SOC) band gap, if nonzero, is less regular because it occurs away from the Γ point and is more dependent on details of the dispersion and inversion energy.

Only the Ae_3BiSb compounds show negative inversion energy when the mBJ correction is included. Sr_3BiAs has very small positive inversion energy (0.06 eV). The rest are normal insulators. Many of these inversion energies, positive or negative, are small enough that they can be manipulated by pressure or strain, with an example discussed in Sec. IV.

The bands of the four compounds we have chosen are shown in Fig. 4, all based on Bi on the A site to provide the largest effect of SOC. Ca_3BiN in Fig. 4(a) provides the reference normal-insulator situation, with a twofold level (A atom $p_{3/2}$) at the VBM and a doublet and a somewhat higher singlet in the lower conduction bands. The bands for the three cases, GGA(SOC), GGA(SOC) + mBJ, and GGA(SOC) + GW_\circ , are aligned at the VBM. The corrections to the valence bands are not very important for our current considerations, but the two corrections are rather small and not necessarily similar. The conduction-band corrections are larger in the region pictured, about 0.5 eV, and similar in the low-energy region that is shown. Comparisons between mBJ and GW corrections have been commented on previously [19].

Figure 4(c) shows the Sr analog, Sr_3BiN . Its gap is smaller, but more interesting is the fact that the conduction-band singlet has dropped close to the doublet. Unexpectedly, the GW_\circ correction has dropped to 0.15 eV, while mBJ remains near 0.5 eV. The corrections in the valence bands remain small, and again, the two corrections are not always similar.

Band inversion occurs for Ca_3BiP shown in Fig. 4(b) due to the conduction-band singlet dropping not only below the doublet but also below the VBM doublet. One crucial result is that the band structure becomes that of a zero-gap semiconductor. Away from Γ the bands hybridize, complicating the process of following the underlying bands. However, the inversion becomes clear when it is noticed that both self-energy corrections raise the Γ GGA(SOC) eigenvalue at -0.3 eV, consistent with conduction eigenvalue character, which is also confirmed by its positive-parity eigenvalue.

This behavior is repeated for Sr_3BiAs , shown in Fig. 4(d), where the band orderings and corrections are somewhat different than in Ca_3BiP and may be easier to follow. Even in GGA(SOC) the low-energy band structure can be quite delicate but becomes more so in the presence of self-energy

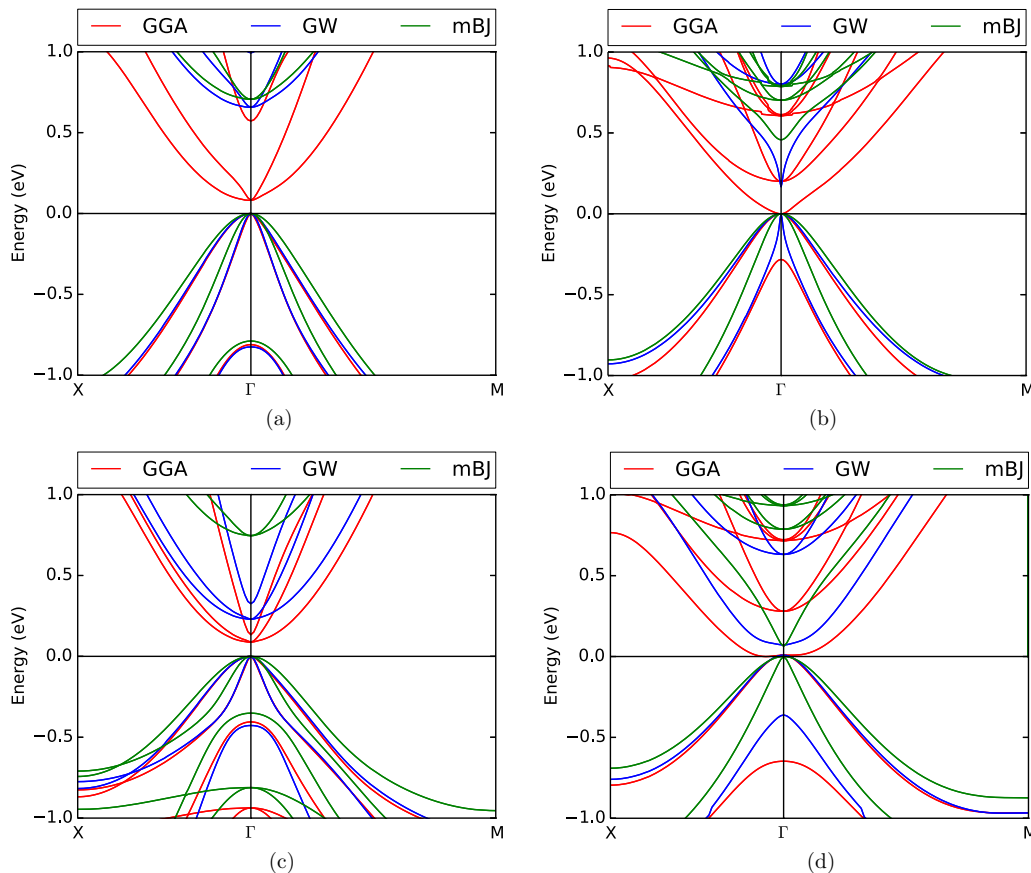


FIG. 4. GGA (red), GW (blue), and mBJ (green) energy bands along X - Γ - M directions for four antiperovskite compounds. All include spin-orbit coupling. (a) Ca_3BiN , (b) Ca_3BiP , (c) Sr_3BiN , and (d) Sr_3BiAs .

corrections. This complex behavior will be explored in more detail elsewhere.

D. Reported antiperovskites

Relatively few of this class of antiperovskite compounds have been synthesized, often without full characterization and only nitrides. Most of these are based on the Ca^{2+} cation. All four $\text{Ca}_3\text{Pn}_A\text{N}$ compounds were reported to be either semiconducting ($\text{Pn}_A = \text{Bi}, \text{Sb}$) or insulating ($\text{Pn}_A = \text{As}, \text{P}$) [3]. Our calculated band gaps from Table I also indicate semiconducting states, as did previous work on some of these members [20] and the Sr and Ba counterparts $(\text{Sr}, \text{Ba})_3(\text{Sb}, \text{Bi})\text{N}$ [21]. When Bi is substituted by the smaller pnictides Sb, As, and P, the band gap increases because, as the electronegativity decreases, the energy level of the p anion relative to the cation level decreases as well.

Structurally, the $\text{Pn}_A = \text{Bi}$ and Sb members of $\text{Ca}_3\text{Pn}_A\text{Bi}$ are cubic, while (presumably) the size mismatch for the smaller ions $\text{Pn}_A = \text{As}$ and P anions led to orthorhombic $Pnma$ distortion [4]. Niewa's review reported $\text{Sr}_3(\text{Sb}, \text{Bi})\text{N}$ as being cubic, as well as $\text{Mg}_3(\text{As}, \text{Sb})\text{N}$ [22], which are not included in our study [5]. In contrast, a hexagonal structure was reported for $\text{Ba}_3(\text{Sb}, \text{Bi})\text{N}$, built on face-sharing rather than corner-linked octahedra. Such a hexagonal structure tends to be favored by compounds containing alkaline-earth-metal species with large radii. Coulomb repulsion between N atoms

in face-sharing octahedra and the resulting distance $d(\text{N-N})$ have been suggested to play a role in stabilizing the structure [5,21]. The $d(\text{N-N})$ for $\text{Ba}_3(\text{Sb}, \text{Bi})\text{N}$ is 3.30 Å, which is sufficiently large to stabilize the hexagonal structure.

Some of these small-gap compounds have been calculated to be promising thermoelectric materials [20,23] with a high thermodynamic figure of merit, viz., $\text{Sr}_3(\text{Sb}, \text{Bi})\text{N}$ [23]. Magnetic susceptibility and electrical resistivity data indicate that the compounds are diamagnetic semiconductors. The optical band gaps of Sr_3SbN and Sr_3BiN are reported to be 1.15 and 0.89 eV, respectively [21].

First-principles calculations have been reported for some of the mentioned compounds, largely to assess specific properties such as their elastic behavior and optical response [24–34]. Our survey should be useful in interpretation of those results by connecting their computed properties to similarities and differences in their electronic structures.

IV. ON THE POSSIBILITY OF TOPOLOGICAL CHARACTER

The Z_2 -invariant ν_0 determines the topological nature of an insulator, and for inversion-symmetric crystals the parity criterion proposed by Fu and Kane [35] determines the topological character. Specifically, the sum of the parities δ_i at occupied states at the time-reversal-invariant momenta

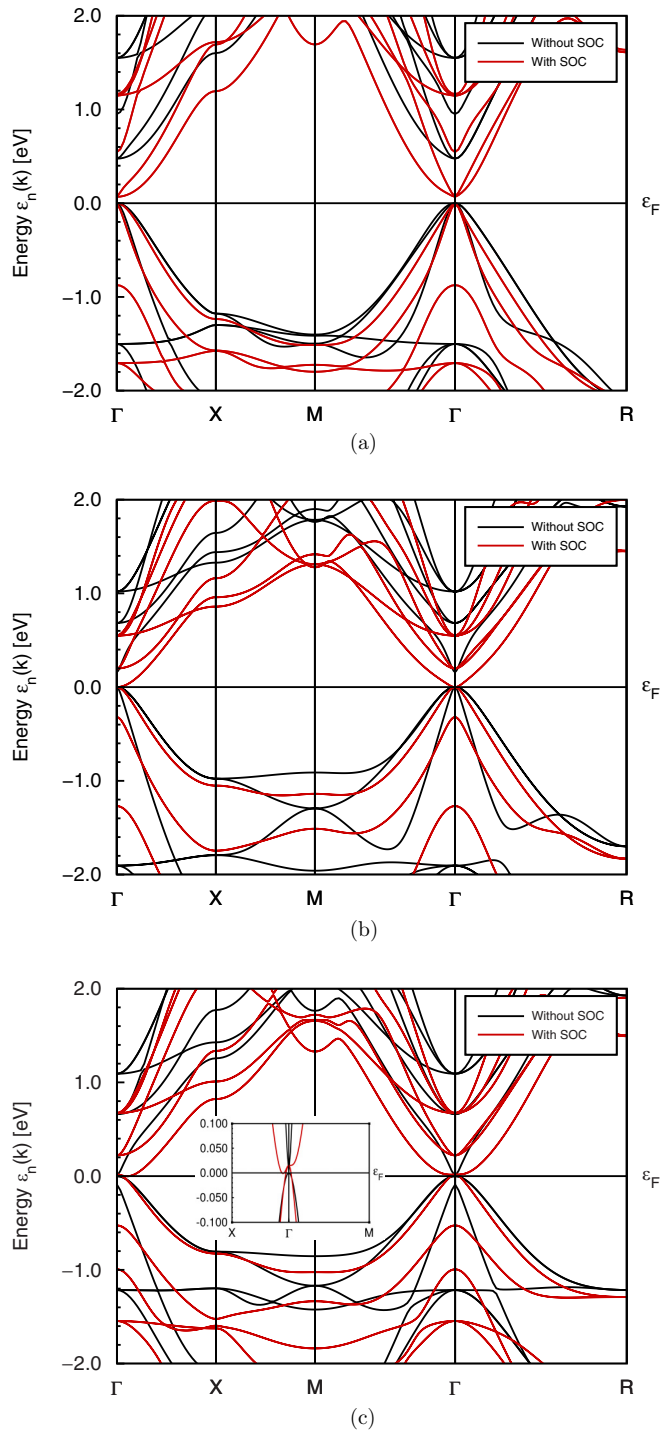


FIG. 5. The $Ae_3Pn_A Pn_B$ antiperovskite compounds can be classified into three categories based on their electronic structure and topological invariants. The electronic band structures of (a) Ca_3BiN , (b) Ca_3BiP , and (c) Sr_3BiN are used as examples of each category, where (a) Ca_3BiN is a normal insulator with small gap, (b) Ca_3BiP is a topological semimetal with CBM and VBM touching, and (c) Sr_3BiP is a topological semimetal with delicate hole pockets, as indicated in the inset.

(TRIMs) determines the primary Z_2 -invariant ν_0 :

$$(-1)^{\nu_0} = \prod_{i=1}^8 \delta_i. \quad (1)$$

By studying Table I it can be seen that the electronic structure and topological nature of these compounds can be classified into three categories: (i) a small gap with a topologically trivial phase occurs, viz., Ca_3BiN in Fig. 5(a). (ii) The VBM and CBM touch at the Γ point with Z_2 indices of (1; 000), like for Ca_3BiP in Fig. 5(b). (iii) There are (usually tiny) electron and hole pockets along high-symmetry lines with Z_2 indices of (1; 000), as in the example of Sr_3BiP in Fig. 5(c).

For the first type, band inversion is not present for the cubic structure, but the application of strain may lead to inversion and a topological material [2]. For the second and third types (highlighted in bold in Table I), the band inversion is induced by SOC of the heavy elements [36]. No gap is opened, however, leaving these systems as topological semimetals. Strain can be used to induce a transition from topological semimetal to topological insulator, provided that the band overlap [especially for type (iii)] is not greater than the effect of SOC.

A case study of Ca_3BiP will be used to demonstrate the role that interplay of SOC and strain plays in band inversion of the second and third classes above. Figure 6 shows the schematic energy-level diagram of Ca_3BiP at the Γ point, along with the bands around Γ for the same conditions. Cubic Ca_3BiP has an energy gap of 0.2 eV. At the Γ point, the valence bands composed of Bi $6p$ characters and P $3p$ characters have negative parities, while the s character of the CBM has positive parity. (There are substantial gaps at all other TRIMs, so their contributions to Z_2 are invariant to all changes and are the same for all of these antiperovskite compounds.) The strong SOC of Bi inverts the s conduction band and the valence Bi $6p$ bands. No gap is opened, however, resulting in a topological semimetal phase.

With a tetragonal compression of 5% along (001), the degeneracy is lifted, and a small gap of 34 meV is produced while maintaining the inverted band ordering. The strain does not violate inversion symmetry but merely splits the degeneracy of the Γ_8^- band at the Fermi level into two sets of Kramers doublets, with odd parity below the Fermi level and even parity above, leaving the parity eigenvalues unchanged. This mechanism is similar to that of α -Sn and HgTe topological insulators [7,35]. Although HgTe does not have inversion symmetry, this II-VI compound can be viewed as adding an inversion-symmetry-breaking perturbation into a group-IV elemental compound, viz., α -Sn (gray tin).

The transition from the topological semimetal state to a topological insulator can also be realized by compressing the lattice parameter c by a few percent, which can be accomplished by growth of thin films on a substrate with the corresponding lattice parameter. As shown in Fig. 7, a small energy band gap with SOC is produced within this range, with a maximum gap of 40 meV occurring at 3% compression. The band parity remains odd within this range but goes back to even at 8% compression. On the other hand, uniaxial expansion along the c axis opens up a gap except along k_z , where a Dirac-like band crossing occurs, producing a topological Dirac semimetal [Fig. 6(f)]. However, not all directions of strain application will open up a gap. For example, applying uniaxial strain along the (111) direction does not open up a gap because the Bi p_x , p_y , and p_z characters still remain equivalent.

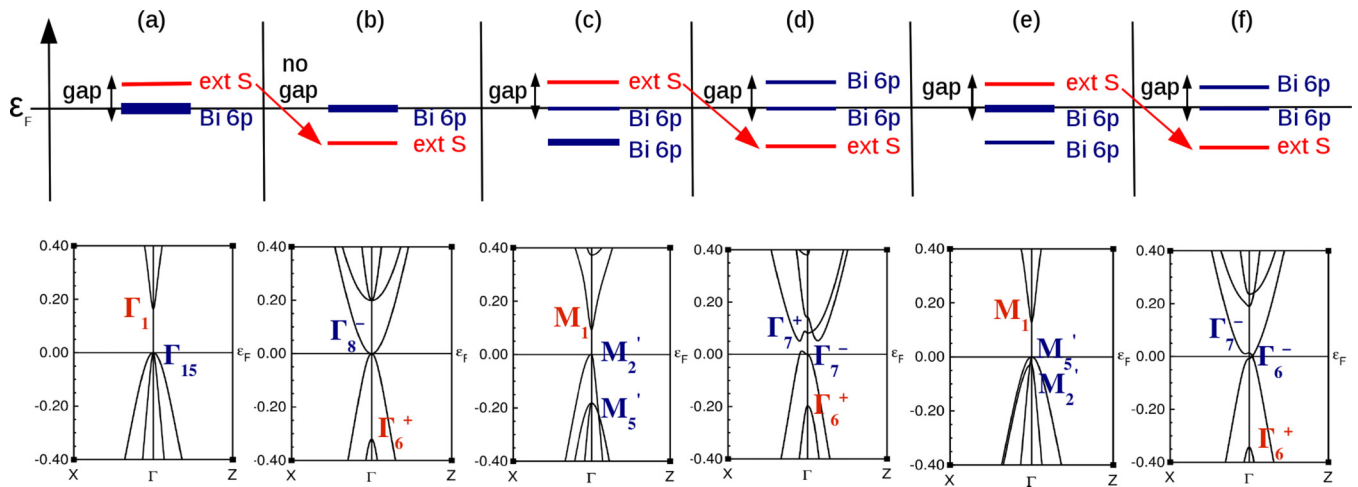


FIG. 6. Top: Schematic energy diagram of Ca_3BiP at the Γ point (a) without SOC, (b) with SOC, (c) with 5% compressive strain and without SOC, (d) with 5% compressive strain and SOC, (e) with 1% expansive strain and without SOC, and (f) with 1% expansive strain and SOC. Ultrafine, fine, and thick lines represent onefold, twofold, and threefold degeneracy (not including spin degeneracy), respectively. Bottom: Band structures along $X-\Gamma-Z$ with irreducible representations given (in Bouckaert-Smoluchowski-Wigner notation) at the Γ point.

V. STRUCTURAL (IN)STABILITY

The oxide perovskite structure is notoriously subject to distortion from the ideal cubic structure for two primary reasons. First, perovskite is not a close-packed structure. Especially, the BO_2 (001) layer (viz., the CuO_2 layer in high-temperature superconducting cuprates) is not: atoms are aligned in rows with an empty site of square symmetry. Second, there is tension between the preferred lattice constants of the BO_2 layer and the AO layer. The mismatch is quantified by Goldschmidt’s ratio, using established ionic radii and quantifying the mismatch as a percentage. It may be expected that these antiperovskites being studied may be subject to similar issues. Unfortunately, these antiperovskites comprise a new class of compounds for which appropriate ionic radii have not been established.

Calculation of the phonon spectrum is commonly used to assess dynamical stability of a compound. Antiperovskites with a N atom at the B site have been studied both experimentally and computationally [4,5,20,21,23–34]. However, B-site cations other than N have not yet been incorporated into this structure. We have calculated the phonon dispersion curves for

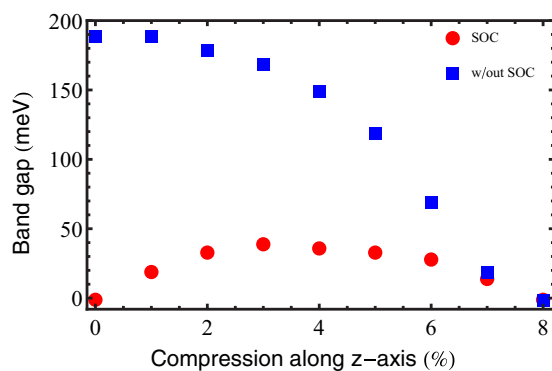
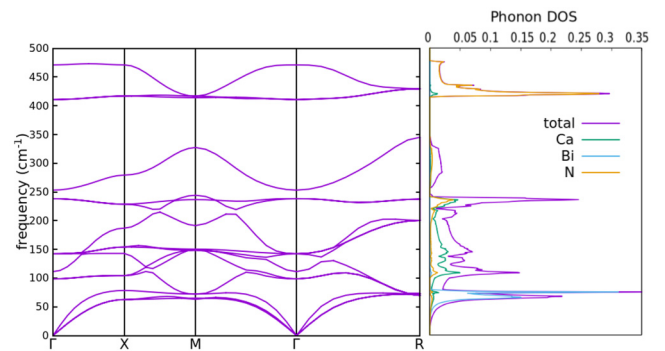


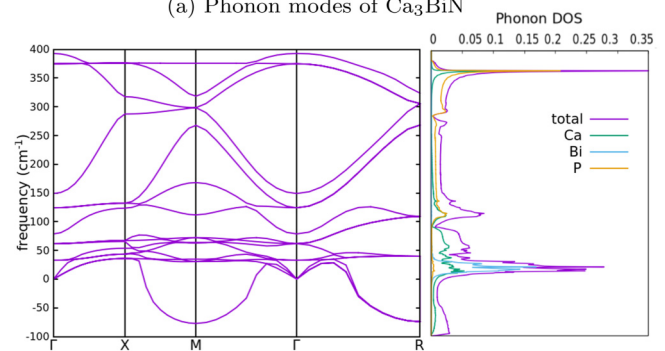
FIG. 7. Band gap of Ca_3BiP versus compression, showing the effect of SOC. Compression along (001) without SOC closes the band gap. When SOC is included, the band gap is closed but then is reopened by strain.

Ca_3BiN and for Ca_3BiP to assess their stability. The results are presented in Fig. 8.

For Ca_3BiN , all frequencies are positive, and the Bi atom dominates the acoustic frequencies up to 75 cm^{-1} . Ca atoms dominate frequencies in the $100\text{--}300\text{-cm}^{-1}$ range, while the light N atom oscillates in the highest-frequency $400\text{--}475\text{-cm}^{-1}$ region. The phonon spectrum of Ca_3BiP is quite different. The



(a) Phonon modes of Ca_3BiN



(b) Phonon modes of Ca_3BiP

FIG. 8. Calculated phonon dispersion of (a) Ca_3BiN and (b) Ca_3BiP . Imaginary frequencies (plotted as negative) indicate structural instability, which is severe for Ca_3BiP for both M and R point rotations.

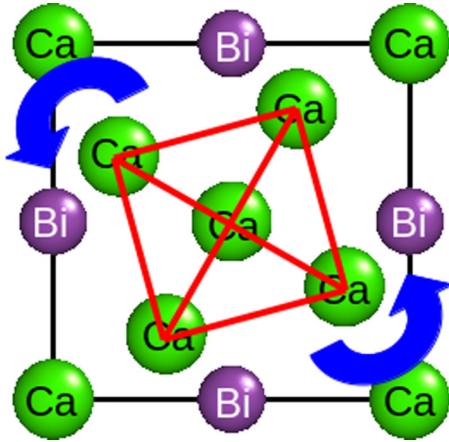


FIG. 9. Structure of distorted Ca_3BiP viewed along the z axis after the Ca octahedron (marked in red) has rotated around the z axis.

overriding feature is the imaginary frequencies around both the M and R points of the zone. The atomic displacements at these points give insight into the structural instability; the unstable modes have Bi + Ca character. At the M point, the Bi and P atoms are fixed, while the Ca atoms rotate around the principal axis; thus, the crystal is unstable to such rotations. Allowing the octahedron to rotate around the z axis as shown in Fig. 9, the energy is lowered by 0.2 eV. The electronic rearrangement due to this distortion leaves Ca_3BiP as a conventional insulator.

Distortion of antiperovskite compounds with heavier Pn_B elements, viz., $Ae_3\text{BiSb}$ with $Ae = \text{Ca}, \text{Sr}, \text{and Ba}$, was studied as well. Distortions from the cubic structure were favored by 0.7–0.8 eV per formula unit. The resulting band structures are those of a Dirac semimetal, hosting Dirac points along the Γ - Z direction, as shown for Ca_3BiSb in Fig. 10. However, applying the mBJ correction widens that gap to around 0.4 eV and leaves band structures in conventional insulator states.

VI. SUMMARY

The stability, electronic structure, and topological aspect of the class of isovalent antiperovskite alkaline-earth pnictide compounds have been studied using DFT. This class with pnictide other than N inside the octahedron is distorted with the octahedron rotated along a principal axis. The electronic structures of these compounds with SOC can be classified into three categories. First, in one common class of the topological

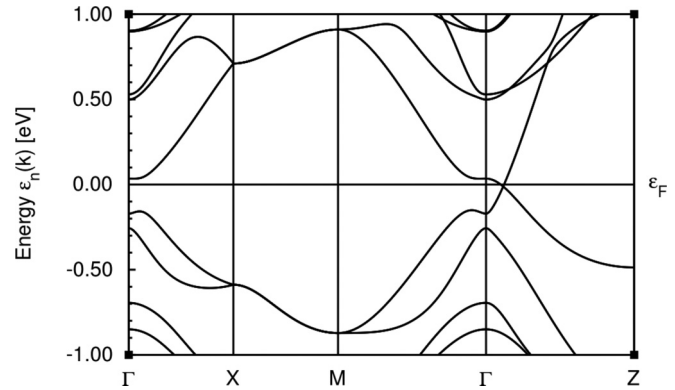


FIG. 10. Band structure of distorted Ca_3BiSb showing the Dirac point along Γ - Z that pins the Fermi level.

aspect the electronic structure is gapped with a topologically trivial phase. The second class is a zero-gap semiconductor with VBM and CBM touching at the Γ point with a Z_2 invariant of $(1; 000)$. In the third class, a semimetal consists of electron or hole pockets with a maximum of 0.1 eV energy and is band degenerate at the Γ point with a Z_2 index of $(1; 000)$. Strain is required to produce a topological insulator. While the first type (e.g., Ca_3BiN) needs both SOC and proper strain to have band ordering inverted [2], the second and third types (e.g., Ca_3BiP and Sr_3BiP) need only SOC to induce the band inversion, giving a Z_2 invariant of $(1; 000)$, but in a topological semimetal state, whereupon compressive strain may produce a transition to a topological insulator. On the other hand, expansive strain may give rise to Dirac semimetals. With proper strain engineering, some compounds may become promising topological insulators and Dirac semimetals, as seen in Ca_3BiP and Sr_3AsP antiperovskite compounds.

ACKNOWLEDGMENTS

We acknowledge useful comments from T. Siegrist and M. Subramanian about pnictide-based antiperovskite and nitride perovskite synthesis. This work was supported by the NSF DMREF program through Grant No. DMR-1534719. Computational data for the compounds in Table I were uploaded to the DOE-supported Materials Project. This research used resources of the National Energy Research Scientific Computing Center (NERSC), a DOE Office of Science User Facility supported by the Office of Science of the U.S. Department of Energy under Contract No. DE-AC02-05CH11231.

- [1] R. Sarmiento-Pérez, T. F. T. Cerqueira, S. Körbel, S. Botti, and M. A. L. Marques, Prediction of stable nitride perovskites, *Chem. Mater.* **27**, 5957 (2015).
- [2] Y. Sun, X. Q. Chen, S. Yunoki, D. Li, and Y. Li, New Family of Three-Dimensional Topological Insulators with Antiperovskite Structure, *Phys. Rev. Lett.* **105**, 216406 (2010).
- [3] M. Y. Chern, D. A. Vennos, and F. J. DiSalvo, Synthesis, structure, and properties of anti-perovskite nitrides Ca_3MN , $M = \text{P}, \text{As}, \text{Sb}, \text{Bi}, \text{Ge}, \text{Sn}, \text{and Pb}$, *J. Solid State Chem.* **96**, 415 (1992).
- [4] M. Y. Chern, F. J. DiSalvo, J. Parise, and J. A. Goldstone, The structural distortion of the anti-perovskite nitride Ca_3AsN , *J. Solid State Chem.* **96**, 426 (1992).
- [5] R. Niewa, Alkaline-earth metal nitrides of the main-group elements: Crystal structures and properties of inverse perovskites, *Z. Anorg. Allg. Chem.* **639**, 1699 (2013).
- [6] D. A. Papaconstantopoulos and W. E. Pickett, Ternary nitrides BiNCA_3 and PbNCA_3 : Unusual ionic bonding in the antiperovskite structure, *Phys. Rev. B* **45**, 4008 (1992).

- [7] Y. Ando, Topological insulator materials, *J. Phys. Soc. Jpn.* **82**, 102001 (2013).
- [8] S. Chadov, X. Qi, J. Kübler, G. H. Fecher, C. Felser, and S. C. Zhang, Tunable multifunctional topological insulators in ternary Heusler compounds, *Nat. Mater.* **9**, 541 (2010).
- [9] S. Zaheer, S. M. Young, D. Cellucci, J. C. Y. Teo, C. L. Kane, E. J. Mele, and A. M. Rappe, Spin texture on the Fermi surface of tensile-strained HgTe, *Phys. Rev. B* **87**, 045202 (2013).
- [10] T. Kariyado and M. Ogata, Three-Dimensional dirac electrons at the fermi energy in cubic inverse perovskites: Ca₃PbO and its family, *J. Phys. Soc. Jpn.* **80**, 083704 (2011).
- [11] J. P. Perdew, K. Burke, and M. Ernzerhof, Generalized Gradient Approximation Made Simple, *Phys. Rev. Lett.* **77**, 3865 (1996).
- [12] K. Koepnick and H. Eschrig, Full-potential nonorthogonal local-orbital minimum-basis band-structure scheme, *Phys. Rev. B* **59**, 1743 (1999).
- [13] A. D. Becke and E. R. Johnson, A simple effective potential for exchange, *J. Chem. Phys.* **124**, 221101 (2006).
- [14] F. Tran, P. Blaha, and K. Schwarz, Band gap calculations with Becke-Johnson exchange potential, *J. Phys.: Condens. Matter.* **19**, 196208 (2007).
- [15] F. Tran and P. Blaha, Accurate Band Gaps of Semiconductors and Insulators with a Semilocal Exchange-Correlation Potential, *Phys. Rev. Lett.* **102**, 226401 (2009).
- [16] H. Jiang, R. I. Gomez-Abal, X. Li, C. Meisenbichler, C. Ambrosch-Draxl and M. Scheffler, FHI-gap: A GW code based on the all-electron augmented plane wave method, *Comput. Phys. Commun.* **184**, 348 (2013).
- [17] H. Jiang and P. Blaha, GW with linearized augmented plane waves extended by high-energy local orbitals, *Phys. Rev. B* **93**, 115203 (2016).
- [18] P. Blaha, K. Schwarz, G. Madsen, D. Kvasnicka, and J. Luitz, *WIEN2k: An Augmented Plane Wave + Local Orbitals Program for Calculating Crystal Properties* (Technische Universität Wien, Vienna, 2008).
- [19] J. A. Camargo-Martínez and R. Baquero, Performance of the modified Becke-Johnson potential for semiconductors, *Phys. Rev. B* **86**, 195106 (2012).
- [20] M. Bilal, S. Jalali-Asadabadi, R. Ahmad, and I. Ahmad, Electronic properties of antiperovskite materials from state-of-the-art density functional theory, *J. Chem.* **2015**, 495131 (2015).
- [21] F. Gäbler, M. Kirchner, W. Schnelle, U. Schwarz, M. Schmitt, H. Rosner, and R. Niewa, (Sr₃N)E and (Ba₃N)E (E = Sb, Bi): Synthesis, crystal structures, and physical properties, *Z. Anorg. Allg. Chem.* **630**, 2292 (2004).
- [22] E. O. Chi, W. S. Kim, N. H. Hur, and D. Jung, New Mg-based antiperovskites PnNMg₃ (Pn=As, Sb), *J. Solid State Commun.* **121**, 309 (2002).
- [23] M. Bilal, Saifullah, M. Shafiq, B. Khan, H. A. R. Aliabad, S. J. Asadabadi, R. Ahmad, and I. Ahmad, Antiperovskite compounds SbNSr₃ and BiNSr₃: Potential candidates for thermoelectric renewable energy generators, *Phys. Lett. A* **379**, 206 (2015).
- [24] K. Haddadi, A. Bouhemadou, and L. Louail, Structural, elastic and electronic properties of the hexagonal anti-perovskites SbNBa₃ and BiNBa₃, *Comput. Mater. Sci.* **48**, 711 (2010).
- [25] M. Hichour, D. Rached, M. Rabah, S. Benalia, R. Khenata, and F. Semari, Structural and elastic properties of antiperovskites XNBa₃ (X=As, Sb) under pressure effect, *Phys. B (Amsterdam, Neth.)* **404**, 4034 (2009).
- [26] D. Rached, M. Hichour, M. Rabah, S. Benalia, H. Rached, and R. Khenata, Prediction study of the structural, elastic, electronic and optical properties of the antiperovskite BiNBa₃, *Solid State Commun.* **149**, 2002 (2009).
- [27] P. K. Jha and S. K. Gupta, First principles lattice dynamical study of the cubic antiperovskite compounds AsNBa₃ and SbNBa₃, *Solid State Commun.* **150**, 1650 (2010).
- [28] I. Ullah, G. Murtaza, R. Khenata, A. Mahmood, M. Muzzamil, N. Amin, and M. Saleh, Structural and optoelectronic properties of X₃ZN (X = Ca, Sr, Ba; Z = As, Sb, Bi) Anti-perovskite compounds, *J. Electron. Mater.* **45**, 3059 (2016).
- [29] K. Bidai, M. Ameri, and I. Ameri, A first-principles study on structural, thermodynamics and elastic properties of XNBa₃ (X=As, Sb) under pressure and temperature effect, *Optik: Intl. J. Light Electron Opt.* **127**, 3150 (2016).
- [30] M. Bilal, I. Ahmad, H. A. R. Aliabad, and S. J. Asadabadi, Detailed DFT studies of the band profiles and optical properties of antiperovskites SbNCA₃ and BiNCA₃, *Comput. Mater. Sci.* **85**, 310 (2014).
- [31] K. Haddadi, A. Bouhemadou, L. Louail, F. Rahal, and S. Maabed, Prediction study of the structural, elastic and electronic properties of ANSr₃ (A=As, Sb and Bi), *Comput. Mater. Sci.* **46**, 881 (2009).
- [32] M. Hichour, R. Khenata, D. Rached, M. Hachemaoui, A. Bouhemadou, A. H. Reshak, and F. Semari, FP-APW+lo study of the elastic, electronic and optical properties for the cubic antiperovskite ANSr₃ (A=As, Sb and Bi) under pressure effect, *Phys. B (Amsterdam, Neth.)* **405**, 1894 (2010).
- [33] M. Moakafi, R. Khenata, A. Bouhemadou, F. Semari, A. H. Reshak, and M. Rabah, Elastic, electronic and optical properties of cubic antiperovskites SbNCA₃ and BiNCA₃, *Comput. Mater. Sci.* **46**, 1051 (2009).
- [34] K. Haddadi, A. Bouhemadou, L. Louail, S. Maabed, and D. Maouche, Structural and elastic properties under pressure effect of the cubic antiperovskite compounds ANCa₃ (A=P, As, Sb, and Bi), *Phys. Lett. A* **373**, 1777 (2009).
- [35] L. Fu and C. L. Kane, Topological insulators with inversion symmetry, *Phys. Rev. B* **76**, 045302 (2007).
- [36] H. Jin, S. H. Rhim, J. Im, and A. J. Freeman, Topological oxide insulator in cubic perovskite structure, *Sci. Rep.* **3**, 1651 (2013).